In Situ Characterization of Protein Corona Formation on Silica Microparticles Using Confocal Laser Scanning Microscopy Combined with Microfluidics

Alessia C. G. Weiss,[†] *Kilian Krüger,*[‡,#] *Quinn A. Besford,*[†] *Mathias Schlenk,*[‡] *Kristian Kempe,*[§] *Stephan Förster,*[‡,#,⊥] *and Frank Caruso**[,†]

[†]ARC Centre of Excellence in Convergent Bio-Nano Science and Technology, and the Department of Chemical Engineering, The University of Melbourne, Parkville, Victoria 3010, Australia

[‡]Physical Chemistry I, University of Bayreuth, Universitätsstraβe 30, 95447 Bayreuth, Germany

[#]JCSN-1/ICS-1, Forschungszentrum Jülich GmbH, Wilhelm-Johnen-Straβe, 52428 Jülich, Germany

[§]ARC Centre of Excellence in Convergent Bio-Nano Science and Technology, and Monash Institute of Pharmaceutical Sciences, Monash University, Parkville, Victoria 3052, Australia

[⊥]Physical Chemistry, RWTH Aachen University, 52074 Aachen, Germany

*E-mail: fcaruso@unimelb.edu.au

KEYWORDS: kinetics, particles, nanoengineering, low-fouling, adsorption

ABSTRACT

In biological fluids, proteins bind to particles, forming so-called protein coronas. Such adsorbed protein layers significantly influence the biological interactions of particles, both in vitro and in vivo. The adsorbed protein layer is generally described as a two-component system comprising “hard” and “soft” protein coronas. However, a comprehensive picture regarding protein corona structure is lacking. Herein, we introduce an experimental approach that allows for in situ monitoring of protein adsorption onto silica microparticles. The technique, which mimics flow in vascularized tumors, combines confocal laser scanning microscopy with microfluidics and allows the study of the time-evolution of protein corona formation. Our results show that protein corona formation is kinetically divided into three different phases: phase 1, proteins irreversibly and directly bound (under physiologically relevant conditions) to the particle surface; phase 2, irreversibly bound proteins interacting with pre-adsorbed proteins, and phase 3, reversibly bound “soft” protein corona proteins. Additionally, we investigate particle–protein interactions on low-fouling zwitterionic-coated particles where the adsorption of irreversibly bound proteins does not occur, and on such particles only a “soft” protein corona is formed. The reported approach offers the potential to define new state-of-the art procedures for kinetics and protein fouling experiments.

INTRODUCTION

Nano- and micro-sized particles are widely studied owing to their potential in drug delivery, therapy, and diagnostics. An important aspect in their development is to establish a fundamental understanding of protein adsorption onto them—upon formation of the so-called protein corona, the particle "synthetic identity" transitions to a "biological identity", subsequently influencing the physiological and therapeutic response of the particles.[1–3] The protein corona is generally described as a two-component system.[4] Proteins with a high affinity for the particle surface form a tightly bound layer, the "hard" protein corona. This layer is surrounded by a protein cloud, often referred to as the "soft" protein corona, wherein rapid dynamic exchange of proteins between the solution medium and particles dominates.[5,6] However, because of the limited number of suitable characterization methods for monitoring and evaluating protein adsorption in detail, it is difficult to clearly define the different layers to confirm the general description used for protein coronas.[7–9] Depending on the characterization method used, the protein corona is described according to either the Gibbs free energy ΔG,[8,10–12] which defines the adsorption and desorption rates of proteins, or binding force[13,14] between the proteins and particle surface. Proteins with a large ΔG have a low probability of desorption and therefore remain associated with the particle surface. These proteins are considered to form the "hard" protein corona. Distinction based on binding forces implies that "hard" protein corona proteins interact directly with the particle surface through long-range, strong protein–surface interactions, whereas proteins in the "soft" protein corona interact with other proteins through short-range, weak protein–protein interactions. Another theoretical distinction is based on the persistence of the protein to remain adsorbed throughout the nanoparticle's journey (i.e. from bloodstream to tissue and past-endocytic environments) as protein corona composition changes during biophysical events.[6–8,15,16] The concept of "persistent" proteins

originates from studies where the "hard" protein corona is used to follow the particle's past.[17–19] It is becoming increasingly important to clearly understand the complex process of protein corona formation, with a focus on the influence of the "soft" protein corona on physiological interactions.[4,7,13,20–24] However, to do so, it is crucial to acquire and understand further details such as the time-evolution of protein corona formation.

Existing techniques for investigating the protein corona can be divided into ex situ and in situ methods. Ex situ approaches study the protein corona after isolation of the particles from the biological environment.[7] This process may change the protein corona composition and may not preserve the "soft" protein corona.[8,25,26] Therefore, such techniques are essentially limited to the analysis of the "hard" protein corona. In contrast, in situ methods monitor the particle–protein complex directly in the incubation solution, allowing for analysis of the "soft" protein corona. Insights on the corona thickness, protein surface affinities and stoichiometries of protein association with, and dissociation from, the nanoparticle surface, as well as the protein structure can be obtained. Commonly used analytical tools include dynamic light scattering,[27,28] fluorescence correlation spectroscopy,[23,25,29] zeta potential measurements,[27,30] circular dichroism spectroscopy,[31,32] Fourier transform infrared spectroscopy,[32] and isothermal titration calorimetry.[33] However, to our knowledge, there is no technique that enables studying the kinetic formation of the entire protein corona in situ and under flow, and further providing a clear distinction in the transition between the "hard" and the "soft" protein corona.

Herein, we introduce the combination of confocal laser scanning microscopy (CLSM) with microfluidics (MF) as a versatile technique to study protein adsorption onto particles. Microfluidic set-ups provide well-defined systems, as important parameters such as channel dimensions and flow rates are precisely controlled. Such well-defined systems facilitate reproducibility of

experimental data and therefore allow standardization of experiments and data reporting.[34,35] By monitoring the increase in fluorescence intensity, which results from the adsorption of fluorescently labeled proteins onto the particles, valuable information about formation kinetics and stability of protein coronas can be obtained. Protein adsorption occurs after milliseconds and continues over several minutes until an equilibrium is reached. Using this technique, three different adsorption regimes are observed, which we hypothesize are linked to the formation of three unique phases. Proteins that adhere with high adsorption rates are directly bound to the particle surface and form the first phase, P^1_{hard}. This layer is surrounded by irreversibly bound proteins that interact with proteins that have already adsorbed, thereby forming the second phase, P^2_{hard}. Both phases belong to the so-called "hard" protein corona and are stable under physiological conditions. A third, loosely attached, and therefore unstable, phase forms the "soft" protein corona (P_{soft}) as the outer layer. The versatility of this approach is further demonstrated by studying the influence of surface chemistry and applied flow rates on protein adhesion. We demonstrate that low-fouling zwitterionic materials prevent the adsorption of irreversibly bound proteins, but that a "soft" protein corona still forms on them. Additionally, by varying the flow rate, we show that protein adsorption kinetics slow down with increasing fluid velocities.

EXPERIMENTAL SECTION

Materials. All chemicals were of analytical grade and used as received without further purification, except for copper(I) bromide (CuBr), which was purified by washing sequentially with glacial acetic acid, absolute ethanol (EtOH), and diethyl ether, followed by drying under vacuum. 2-Hydroxyethyl methacrylate (HEMA) was passed through an aluminum oxide column prior to polymerization to remove the inhibitor. High-purity water (Milli-Q water) with a resistivity of >18.2 MΩ cm was obtained from an inline Millipore RiOs/Origin water purification system

(Millipore Corporation, Massachusetts, USA). Device fabrication was carried out using a Sylgard®184 silicone elastomer and the corresponding curing agent from Dow Corning (Michigan, USA). Silicon wafers (diameter 3 in.) were obtained from Si-Mat Silicon Materials (Germany). Developer mr-DEV 600 and photoresists Nano^{TM} SU-8 50/SU-8 100 were purchased from MicroChem Corporation (Massachusetts, USA). Silica particles with an average size of 16.4 μm (isoelectric point (IEP) 2) were obtained from microParticles GmbH (Germany). Cy3- and Cy5-labeled HSA were obtained from Nanocs (Boston, USA) (IEP 5.3). Dulbecco's phosphate buffered saline (DPBS) and NaOH pellets (97%) were purchased from Aldrich (Missouri, USA). Silica particle functionalization was carried out using (3-aminopropyl)triethoxysilane (APTES, 98%), ammonia (NH_3, 28–30%), pyridine (anhydrous, 99.8%), tetrahydrofuran (THF; anhydrous, 99.9%), and α-bromoisobutyryl bromide (98%), which were all purchased from Aldrich. For the surface-initiated atom transfer radical polymerization (SI-ATRP, HEMA (97%), *N*,*N*,*N*′,*N*″,*N*″-pentamethyldiethylenetriamine (PMDETA, 99%), 2-methacryloyloxyethyl phosphorylcholine (MPC), CuBr (98%), and nitric acid (70%) from Aldrich were used. Fluorescence labeling was carried out using AF488-*N*-hydroxysuccinimide (NHS) purchased from Thermo Fisher (Victoria, Australia) and dimethyl sulfoxide (DMSO) (anhydrous, >99%) that was obtained from Aldrich. Albumin from human serum (lyophilized powder, >96%), purchased from Aldrich, was used for protein corona formation.

Fabrication of MF Devices. The MF chips were prepared according to a modified literature method to mimic the in vivo environment.[36,37] A linear channel design (for the static in situ studies) and a cross-shaped mixer geometry (for the dynamic in situ studies) were used, both with dimensions of 250 μm × 150 μm (height × width) for the main channel. Structures were designed using the AutoCAD 2013 (Autodesk) software. This network was printed on a photomask foil

using a soft photographic emulsion gel. To replicate this design onto a silica wafer, spin-coating cycles of a negative epoxy-based photoresist (SU-8) were applied using a mask aligner (Süss MicroTec). An ~100-µm thick layer was obtained. Soft baking (65 °C, 10 min) steps and UV patterning were performed after each spin-coating step by placing the mask onto the wafer and exposing it to UV light. Unexposed photoresist was removed using developer prior to a final hard baking (95 °C, 30 min) step. Soft lithography was performed by pouring a 10:1 w/w mixture of polydimethylsiloxane (PDMS) base and curing agent onto the silicon master. After degassing for 45 min in a desiccator and subsequent drying for 2 h at 75 °C, the replicate was removed from the master, and inlet ports for fluids were added. To obtain a three-dimensional (3D) channel structure, two PDMS devices were sealed together after plasma activation (air plasma, 5 min) and dried overnight at 35 °C.

Immobilization of Silica Particles for Static Experiments. The silica particles were immobilized in the channel prior to in situ measurements. The particles were first washed with DPBS via repeated centrifugation (1000 *g*, 1 min, 3×) and resuspension steps and subsequently injected into the channel (5 µL concentrated particle stock solution) with a pipette. The solution of the particle dispersion was then allowed to evaporate overnight at 20 °C, resulting in immobilized silica particles. A particle monolayer was obtained by injecting DPBS (10 µL) into the channel to remove excess silica particles.

MF–CLSM Static Experiments. In situ experiments for protein corona formation were carried out by combining CLSM with MF. CLSM images were taken using a Leica TCS SP8 equipped with HCX PL FLUOTAR 5×/0.15 DRY, HCX PL FLUOTAR L 20×/0.40 DRY and 40×/0.60 DRY, as well as Fluotar VISIR 25×/0.95 WATER, HC PL APO CS2 63×/1.20 WATER and HC PL APO CS2 63×/1.30 GLYC objectives. The set-up was also equipped with 405-, 488-, 514-,

552-, and 638-nm lasers, two photomultipliers (PMTs), one transmission photomultiplier (PMTtrans), and an ultra-sensitive hybrid detector. Confocal two-dimensional (2D) images were obtained with an ultra-fast resonance scanner (12,000 Hz) in the *x*–*y* image scan mode. The 638-nm laser was set to 95% with a gain of 500 V for PMT2 and 230 V for PMTtrans. The detection range was set to 660–749 nm. For the measurements, the 3D PDMS MF device was placed on top of a standard glass slide and located under the CLSM microscope. HSA–Cy5 solution in DPBS with a concentration of 0.2 mg mL^{-1} was injected via syringe pumps (Nemesy, CETONI GmbH) equipped with gas-tight Hamilton syringes. This concentration was chosen on the basis of the fluorescence intensity and the detection limits of the instrument. The devices were connected to the syringes via Original-Perfusor lines (Type IV-Standard; B. Braun Melsungen AG, Germany) and medical grade polyethylene microtubings (0.38 mm inner diameter × 1.09 mm outer diameter; Scientific Commodities Inc., Arizona, USA). The applied flow rate was 600 µL h^{-1}. CLSM images were taken before the protein solution was injected into the channel, every ~0.8 s for the first 60 s, and every 30 s from 1.30 to 300 s. From 360 up to 600 s, images were taken every 60 s. A 120 s time interval was applied from 720 to 1200 s. The time interval changed to 300 s between 1500 and 3600 s. The last image was taken after 5400 s. A standard fluorescence curve was constructed as a function of HSA–Cy5 bulk concentration, which showed linear correlation of fluorescence intensity with protein concentration (Figure S1).

MF–CLSM Dynamic Experiments. For the dynamic in situ imaging, the same set-up as that for the static measurements was used. However, a cross-shaped mixer was used as the particle and protein solutions were injected simultaneously. *Z*-scan series were taken in the *x*–*y*–*z* mode and reconstructed by LAS X (Version 2016) software. The focus was adjusted to be at the bottom and top of the MF channel (93.52–85.63 µm) with an increment of 4.71 µm. For the coating

experiments, both the 552-nm and 638-nm lasers were used to detect HSA–Cy3. Both laser intensities were set to 95% with PMT1 = 600 V, PMT2 = 500 V, and PMT_{trans} = 230 V. Detection ranges were 564–620 nm for HSA–Cy3 and 660–749 nm for HSA–Cy5. The particle solution (5 wt% in DPBS) was injected into the middle channel, and the protein solutions (0.2 mg mL^{-1} in DPBS) were injected into side channels. Flow rates were kept constant for all three channels (20,000 μL h^{-1} for initial injection, measurements were taken with an applied flow rate of 500 μL h^{-1} per channel). Particle concentration was measured on a flow cytometer (Apogee Micro Flow cytometer).

Protein Corona Stability Measurements. The MF–CLSM static set-up was used for the stability measurements. Studies were conducted after protein corona formation (which occurred within 90 min) with HSA–Cy5 on bare silica particles. DPBS was injected into the channel with a constant flow rate of 600 μL h^{-1} for 5 min following injection of concentrated NaOH solution (17.6 M).

CLSM Data Analysis. CLSM images were analyzed using ImageJ processing software. Particle fluorescence intensity was averaged over 10–12 different particles per data set (Figure S2). Particles were randomly chosen, however, with no overlap with each other and close to the area of background measurement. For the intensity measurements, the following assumptions were made: (1) background intensity is constant throughout the channel; (2) background intensity is constant over the area of one particle; (3) photobleaching is negligible, as exposure times are <1 s; and (4) laser intensity and detection signal are constant throughout the experiment. Standard deviations were calculated with 95% confidence intervals. Background correction, including protein solution and PDMS inner channel walls, was carried out by measuring the fluorescence intensity at different areas and subtracting the average value from the particle fluorescence intensity. Note that images

were excluded from analysis if undissolved proteins (very high fluorescence intensity) were present in the selected areas for the intensity measurements. Furthermore, normalization of fluorescence intensity was not performed to the highest measured value but to an average value of the highest 10–15 values. This method was chosen to minimize intensity fluctuations and therefore to obtain a more accurate value of the final (plateau) particle intensity. This led to a further exclusion of values for linearization, as $\ln(1 - I)$ is only defined for $I < 1$.

Poly(2-methacryloyloxyethyl phosphorylcholine (PMPC) Coating of Silica Particles. To attach ATRP initiator groups to the surface of the non-porous silica particles, the surface was amino-functionalized. The silica particles (300 mg) were first dispersed in EtOH (4.2 mL). Ammonia (210 µL) and APTES (210 µL) were then added to the suspension and stirred overnight at 20 °C. The volume ratio of EtOH/ammonia/APTES was fixed at 1:1:20. The APTES-modified silica particles were washed via repeated centrifugation (1000 *g*, 1 min) and resuspension steps, first in EtOH (2×) followed by Milli-Q water (2×). The washed particles were then reacted with α-bromoisobutyryl bromide for initiator attachment. A volume ratio of SiO_2-NH_2/THF/α-bromoisobutyryl bromide of 1:15:3 was used. The particles were dispersed in anhydrous pyridine (200 µL) and THF (anhydrous, 4.5 mL). After the addition of α-bromoisobutyryl bromide (900 µL), the suspension was stirred overnight at 20 °C. Purification was performed by washing with EtOH (1000 *g*, 1 min, 2×) and Milli-Q water (1000 *g*, 1 min, 2×). Particles were stored suspended in EtOH in the fridge (8 °C). SI-ATRP was conducted exclusively under strict oxygen exclusion. A molar ratio of the reactants of silica@ATRP/monomers/CuBr/PMDETA of 1:1000:2:2 and a monomer ratio of MPC/HEMA of 90:10 were used. In a Schlenk flask, the monomer mixture (1000 mg, 3.38 mmol MPC, 44 mg, 0.38 mmol HEMA), ATRP initiator-functionalized silica particles (2 mL of 150 mg mL^{-1} stock solution in EtOH), and PMDETA

(1.17 mg, 0.0077 mmol) were dissolved in EtOH (5 mL). The reaction mixture was degassed by three freeze–pump–thaw cycles before CuBr (1.1 mg, 0.0077 mmol) was added, and polymerization was started by heating the mixture to 50 °C. After 20 h, the reaction was quenched by cooling the mixture to 20 °C and exposing it to air. Purification was performed by repeated centrifugation (1000 *g*, 1 min) and resuspension steps using nitric acid (1 M, 1×), 10% pyridine/EtOH (1×), and EtOH (3×) as suspension media. Based on previous studies that show that the monomer ratio prior to polymerization matches that in the polymer,[38,39] we assume that the product particles have a monomer ratio that matches that of the reaction monomer ratio of MPC/HEMA of 90:10. The particles were stored in EtOH in the fridge (~8°C).

HSA Coating of Silica Particles. Albumin coating of the silica particles was performed by immersing the silica particles (100 mg dispersed in 200 µL DPBS) in the protein solutions for 24 h at 20 °C under constant shaking. A protein concentration of 1 mg mL^{-1} in DPBS was used. For fluorescently labeled proteins (HSA–Cy5), a concentration of 0.2 mg mL^{-1} was used. Purification was performed by isolating the particles through centrifugation (1000 g, 1 min) and resuspending them in DPBS. This step was repeated thrice to remove all unbound proteins. Particles were stored in the fridge (~8 °C).

Particle Characterization. Thermogravimetric analysis was conducted on a TGA/SDTA 851 from Mettler Toledo in an air atmosphere. The samples were heated from 30 to 1000 °C at a heating rate of 10 °C min^{-1}. Fluorescence microscopy images were taken with an Olympus IX73 microscope (10× objective, Olympus) equipped with a Nikon D7000 camera. To visualize the PMPC-coated particles, the latter were labeled with NHS-activated Alexa Fluor (AF488-NHS). The particles were dispersed in DMSO (anhydrous, 200 µL), and 5 µL of AF488-NHS (1 mg mL^{-1} in anhydrous DMSO) was added. After 2 h at 20 °C under constant shaking, unreacted dye was

removed by repeated centrifugation (1000 *g*, 1 min) and resuspension steps in Milli-Q water (3×). To visualize the HSA-coated particles, fluorescently labeled HSA–Cy5 was used, instead of non-labeled HSA.

High-Speed Camera Imaging. High-speed camera imaging was performed using a Phantom v1612, Vision Research system. Imaging was performed using a fluorescence microscope IX73 (Olympus Co.) equipped with a UPlanFL N 10× objective and a U-LH100HG mercury lamp. An intense, focused light source allowing exposure down to 2 μs was used. Data analysis was performed using Phantom Control software (version 9.2675.2-C) from Vision Research Inc. Snapshots were selected from the whole image sequence and analyzed with ImageJ software, as described in the CLSM data analysis. The same MF set-up as that for the dynamic MF–CLSM measurements was used.

Optical Waveguide Lightmode Spectroscopy (OWLS). OWLS measurements were performed with an OWLS 210 instrument (MicroVacuum, Budapest, Hungary) programmed with Biosense 2.6 software. Measurements were performed on silica sensor chips that were washed with ethanol and Milli-Q water (3× each), before drying under nitrogen followed by oxygen plasma cleaning. The optical properties of the sensor chips were determined in air, before allowing the sensor chips to equilibrate for 60 min in DPBS. Measurements were performed at 23 °C, and HSA samples were only injected once the system had stabilized so that the change in signal (both n_{TM} and n_{TE}) with time was less than 10^{-8}.

RESULTS AND DISCUSSION

Microfluidic Set-Up. Real-time monitoring of protein corona formation was conducted using CLSM in combination with MF. Microfluidic devices enable in situ monitoring as (1) transparent polymers, such as PDMS, are used to make the device, (2) their dimensions are in a size range that

allows them to fit a standard microscope slide, and (3) they provide a dynamic environment through connection to syringe pumps.[36] 3D PDMS chip fabrication was realized using soft lithography.[37,40] The photolithographic master was fabricated via repeated spin-coating and UV exposure steps with subsequent development and removal of uncured photoresists. The resulting microchannel structure was replicated by PDMS. 3D channel networks were obtained by bonding two devices through air plasma activation. Scheme 1a shows an illustration of the experimental set-up used for static incubation. A linear channel design was employed with one inlet port and one outlet port. Channel dimensions (250 µm × 150 µm, height × width) were designed to mimic fluid flows in vascularized tumors.[41,42] For our studies, non-porous silica microparticles with an average diameter of 16 µm were used as a model system, as they have been widely tested in numerous applications and used in consumer products.[43] As a model protein, fluorescently labeled (cyanine 5, Cy5) human serum albumin (HSA, the most abundant protein in human plasma) (HSA–Cy5) was used.[44] The particles were immobilized in the microfluidic channel by injecting the particle dispersion into the channel and allowing the liquid to evaporate. HSA–Cy5 was subsequently pumped through the channel in a controlled manner via syringe pumps. Protein corona formation was monitored in real time by CLSM, wherein increases in fluorescence intensity correlate to protein adsorption (Scheme 1b). Our approach is conceptually similar to a recent study that used fluorophore-labeled proteins to map the spatial distribution of adsorbed proteins on silica nanoparticles.[45] In our study, quantitative data such as adsorption rates and time spans per phase could be obtained by averaging the increase in fluorescence intensity over 10–12 particles. These data provide valuable information about the time-evolution of protein adhesion. This allows us to distinguish between the different layers and enables comparison over a wide range of parameters such as different surface chemistries, flow rates, and protein concentrations. To better represent an

in vivo environment, we further developed an approach that extended the static set-up to a dynamic system (Scheme 1c,d). Using a cross-shaped mixer channel design with three inlets and one outlet port, particles were hydrodynamically focused in the central stream and surrounded by a fluorescently labeled protein solution.

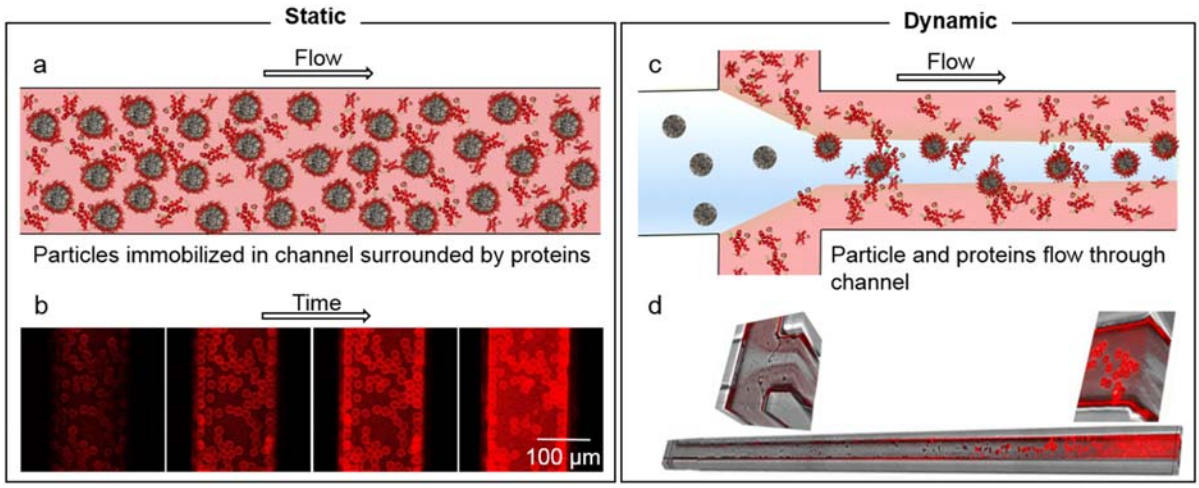

Scheme 1. Schematic of the microfluidic set-ups used for in situ observation of protein corona formation under static and dynamic conditions. (a) Silica particles are immobilized in a 3D microfluidic channel with a fluorescently labeled protein solution (HSA–Cy5) pumped through the channel. (b) Protein corona formation is monitored under real-time conditions by CLSM. The scale bar corresponds to all four images. (c) A 3D PDMS chip with a cross-shaped mixer geometry is used to focus the silica particles in the central stream and surround the particles with a fluorescently labeled protein solution. (d) Protein corona formation is monitored by 3D CLSM images created by *z*-scans through the channel. Near the channel entrance, only fluorescence from the protein solution is detected. As the solution flows toward the channel exit, the particles are coated with the fluorescently labeled proteins and are therefore visible under CLSM.

Protein Incubation under Static Conditions. Measurements were performed under a constant flow rate of 600 µL h^{-1} with a protein concentration of 0.2 mg mL^{-1}. Figure 1 shows the

quantitative data obtained from the CLSM measurements. Figure 1a displays CLSM images (representative for all measurements) captured at different incubation times. The fluorescence intensity increased with increasing incubation times, indicating the formation of a protein corona. Figure 1b confirms the increase in fluorescence intensity (*I*) and plateaus after 190 ± 62 s (Table 1). We assume that the density of HSA–Cy5 adsorbed on the particle surface decreases as a function of layer thickness (i.e. in going from the hard to the soft corona), meaning that the possibility of fluorophore self-quenching is not expected to occur for the latter time series data.

To further analyze the data, linearization based on Equations S1–S3 was performed (Figure 1c). The graphs show three different regimes, denoting three different phases of adsorption ("down (P^1_{hard})–plateau (P^2_{hard})–down (P_{soft})"). Within the first 39 ± 6 s, protein adsorption occurs rapidly, as is evident from the steep increase in fluorescence intensity (Figure 1b). Afterwards, over 46 ± 20 s, the adsorption plateaued (Figure 1c). From 90 s onward, protein adsorption continued again until a final state of equilibrium was reached (Figure 1b). The third phase occurred after 85 ± 26 s. To quantify the data, we further calculate a characteristic time τ for exponential growth from the negative slopes m of the regression lines, as $-m = \frac{1}{\tau}$ applies (Table 1). τ is defined as the characteristic time in which the intensity reaches 63% of its upper limit and is therefore linked to adsorption rates (Equations S4–S13, Figure S3). Note that the applied fit model for linear regression lines is not valid for non-transformed *y* values (that is plateaus) and was therefore not performed. The plateau is indicated by the grey boxes in Figure 1c and Figure 1d. The first phase (P^1_{hard}) displayed the highest adsorption rates owing to strong particle–protein interactions. In the last phase, which we refer to as the region where the "soft" protein corona forms, protein adsorption was 3 times slower when compared with that in the initial phase (P^1_{hard}). We hypothesize that proteins that make up "soft" protein corona are more loosely attached and form a

protein “cloud”. Population–balance models, which state that protein–protein interactions are weaker than protein–surface interactions, and therefore the adsorption rates slow down for subsequent phases, are consistent with the observed three-fold decrease in protein adsorption.[46] However, this theory is in contrast with so-called cooperative effects,[47] which claims that proteins are more likely to adsorb if other proteins are (pre-)adsorbed.

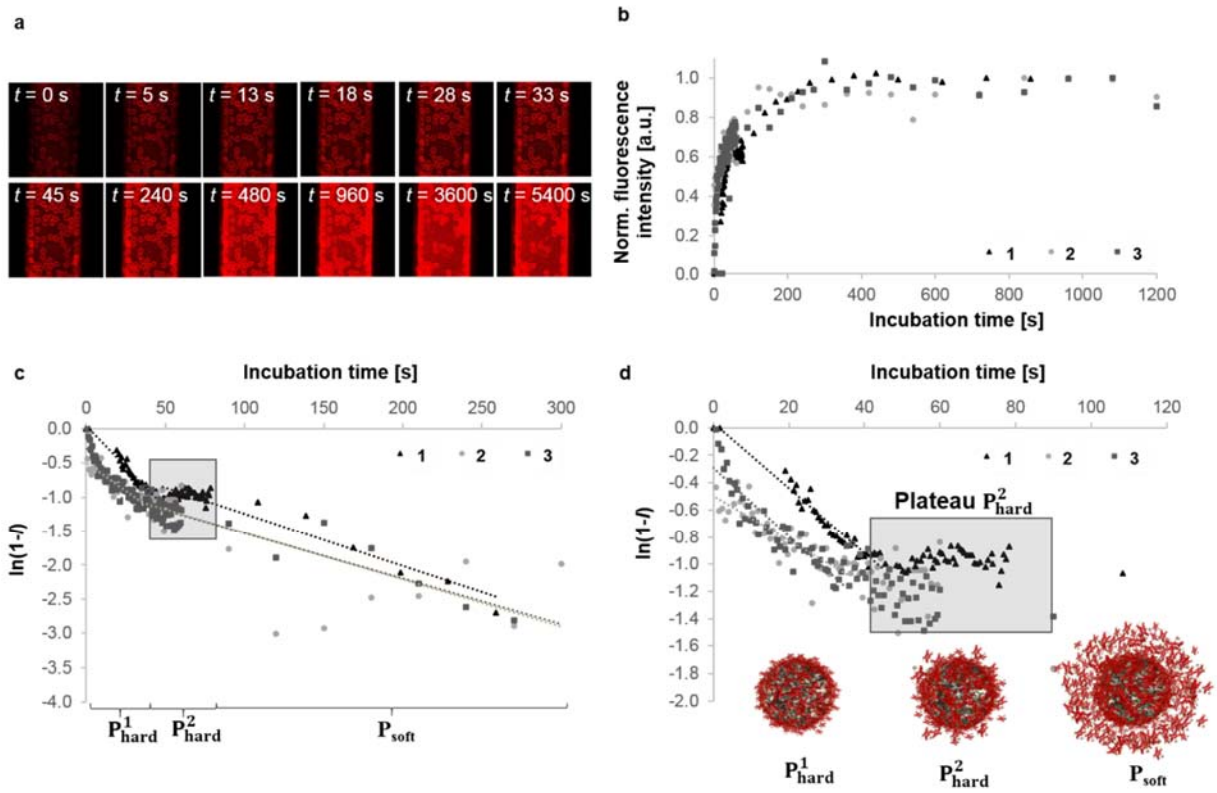

Figure 1. Kinetics of protein corona formation around silica particles for static particle conditions. A constant flow rate of 600 µL h^{-1} and a HSA–Cy5 concentration of 0.2 mg mL^{-1} were used in all experiments. (a) Representative raw data, obtained from 2D CLSM imaging, depicting changes in fluorescence intensity of the particles as incubation proceeds. (b) Normalized particle fluorescence intensity (*I*) as a function of incubation time (with background correction). The experiment was carried out in triplicate (1, 2, 3). (c) Linearized plots of the data plotted in (b) with respective linear fits (dashed lines). (d) Enlarged version of the linearized data, focusing mainly on the first two

phases of adsorption (P^1_{hard} and P^2_{hard}). R^2 values, which indicate goodness-of-fit, and the respective equations for the regression lines are summarized in Table S1 (Supporting information). Full time data are shown in Figures S4 and S5 (Supporting information).

Table 1. Experimental Data for Bare Silica Particles Coated with HSA–Cy5, Obtained from Figure 1

Replicate no.	Time span P^1_{hard} [s]	Time span P^2_{hard} [s]	Time span P_{soft} [s]	τ_{P1} [s]	τ_{soft} [s]	Plateau [s]
1	46	60	5292	42	130	240
2	36	23	5340	61	145	120
3	35	54	5310	40	149	210
Average	39 ± 6	46 ± 20	5314 ± 24	48 ± 12	141 ± 10	190 ± 62

The results summarized in Table 1 also show the reproducibility of the experimental approach used. Both the time spans per phase and the calculated rates for active adsorption steps (P^1_{hard} and P_{soft}) were within the range of the measurement errors.

The adsorbed mass of HSA on silica was probed through optical waveguide lightmode spectroscopy (OWLS). Though OWLS does not provide the resolution required to adequately sample the transitions between P^1_{hard} and P^2_{hard}, the method allows quantification of the adsorbed mass of protein. A sample of pure HSA in DPBS buffer (1 mg mL^{-1}) was injected at a flow rate of 600 μL min^{-1} onto a planar silica substrate, and the final adsorbed mass was calculated to be 1.65 ± 0.073 mg m^{-2} (Figure S6). Recent modelling of orientationally dependent HSA adsorption on silica substrates has determined that the maximum monolayer coverage of irreversibly bound HSA

is 1.4 mg m^{-2}, depending on pH and ionic strength.[48,49] This maximum coverage is in reasonable agreement with our calculated surface coverage (1.65 mg m^{-2}). The difference in the protein adsorbed amount could be indicative of the loosely associated soft corona. Furthermore, by comparing the fluorescence of the HSA–Cy5-coated silica particles that have been purified (by centrifugation and washing) to the standard fluorescence curve of bulk HAS–Cy5 (Figure S1), and with knowledge of the concentration of particles, it is possible to derive the average protein coating amount. Using this approach, we calculated a HSA–Cy5 surface coverage of 1.28 ± 0.28 mg m^{-2}, which is in close agreement with the OWLS data, where the difference between these values possibly being due to the loosely associated proteins being removed through the washings steps. Plotting the fluorescence data from Figure 1b against the OWLS data (Figure S6) demonstrates linearity over the same adsorption time (Figure S7), showing consistency between the two methods. The broad agreement of the data from these experiments suggests that the possibility of fluorescence self-quenching between adjacent adsorbed proteins does not significantly affect our results on the adsorption of HSA–Cy5 proteins on the microparticles.

To further understand the different binding forces, we monitored the time-evolution of fluorescence intensity in a physiologically relevant solution (DPBS) (Figure 2) following formation of the protein corona.

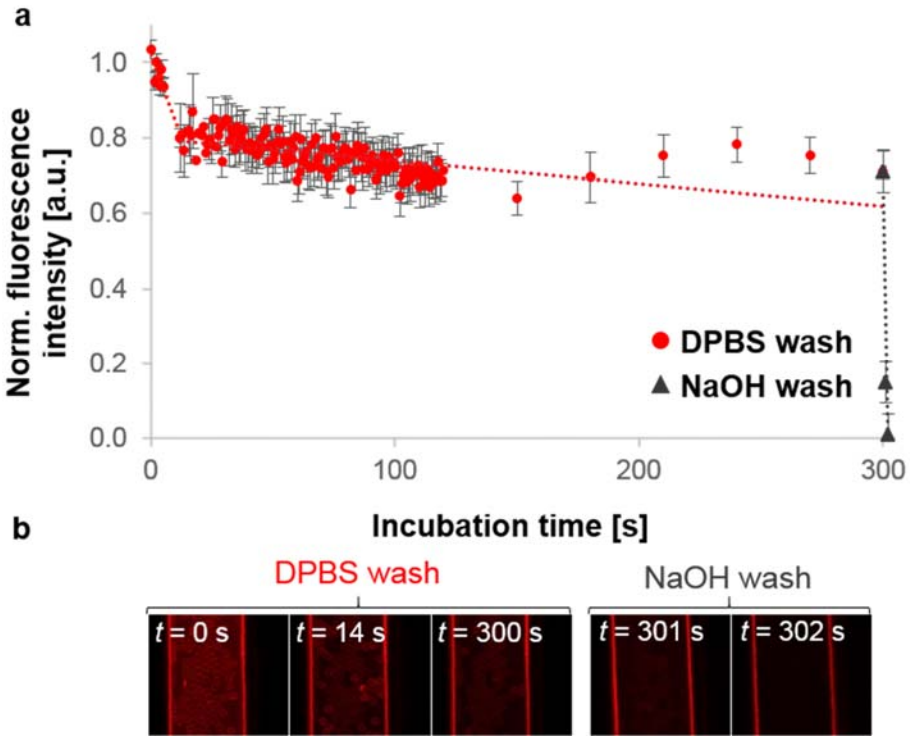

Figure 2. Desorption study in DPBS and NaOH. (a) Normalized particle fluorescence intensity plotted as a function of incubation time (with background corrections) with respective linear fits. After protein corona formation (which occurred within 90 min), DPBS was pumped through the channel for 300 s, followed by concentrated NaOH (17.6 M). (b) Representative raw data, obtained from 2D CLSM imaging, depicting changes in fluorescence intensity of the particles as incubation proceeds. R^2 values, which indicate goodness-of-fit, and the respective equations for the regression lines are summarized in Table S2.

Protein desorption was induced by washing the particles with DPBS. The desorption profile is shown in Figure 2. The steep decline within the first 13 s (crossover of the DPBS-related regression lines (red)) represents desorption of reversibly bound proteins. Afterwards, protein desorption slowed down and reached equilibrium (the fluorescence intensity decreased on average by ~10% over 300 s). These results agree with our theory on the formation of a weakly bound protein layer

(P_{soft}) and the presence of irreversibly bound proteins, which are kinetically subdivided into P^1_{hard} and P^2_{hard} based on the different phases observed in Figure 1c. Note that the local maximum at 240 s is an artefact (Figure 2), as the fluorescence intensity of the particles was lower than the background intensity. Over time, proteins desorbed from the particle surfaces; however, they remained adsorbed onto the PDMS wall. This also explains the low R^2 value obtained for the second phase (13–300 s) of DPBS incubation (Table S2). A final washing step was performed using concentrated NaOH solution to confirm that irreversibly bound proteins remain adsorbed under physiologically relevant conditions but desorb in a strong basic environment. As the fluorescence intensity decreased to 15% of the initial intensity within the first second of the final wash and became undetectable after 2 s, it was evident that strong alkaline conditions removed the adsorbed proteins. Overlaid fluorescence and bright-field microscopy images confirmed that the strong alkaline conditions did not dissolve the silica particles within the time period studied (Figure S8).

Based on our data, we suggest a three-phase model comprising a first layer of tightly bound proteins that interact directly with the particle surface and a second layer consisting of proteins that interact mainly with pre-adsorbed proteins in the first layer. Both layers are irreversibly attached (under physiologically relevant conditions) and therefore form part of what is currently known as the "hard" protein corona.

Assignment of P^1_{hard} and P^2_{hard} to the "hard" protein corona is based on our previous results where the protein corona was studied using ex situ techniques.[39] A three-phase protein corona has also been proposed by Sakulkhu et al. by applying liquid chromatography mass spectrometry.[18] In that study, the protein corona, which was formed on superparamagnetic iron oxide nanoparticles, was categorized according to its structure: soft, hard, and tightly bound, which is similar to a more

recent study by Zhang et al., where a three-phase protein corona was observed on silica nanoparticles.[50] In that study, the three-phase corona was concluded from protein adsorption at saturation (i.e., post-corona formation). In contrast to the three-layer system, other groups have reported on a two-time-scale dynamic of protein corona formation: an initial strongly bound monolayer and a subsequent weakly bound layer.[12,23,33]

To further observe protein corona formation at very small time scales (e.g. 0.5 s), we connected the microfluidic set-up (equipped with a cross-shaped mixer channel design) to a high-speed camera (Figure S9). This combination allowed us to gain insights about protein–particle interactions on a millisecond time scale. The microfluidic set-up provides defined fluid flows and accurate interfaces between two fluids, which help characterize protein corona formation. Preliminary studies regarding visualization were carried out to confirm the effectiveness of this set-up (Figure S10).

Protein Incubation under Dynamic Conditions. To study the time-resolved stability of adsorbed proteins under flow, silica particles were precoated with Cy5-labeled albumin proteins (red fluorescence). Protein corona formation was achieved by incubating the particles with HSA–cyanine 3 (Cy3) (green fluorescence) under flow (Figure 3). Initial flow rates were set to 20,000 μL h^{-1} to obtain controlled fluid flows and reduced to 500 μL h^{-1} for imaging. We note that our set-up does not account for incomplete mixing due to laminar flow along the channel; however, given the relatively high concentration of labeled protein (0.2 mg mL^{-1}) and high initial flow rate, we assume that laminar flow effects do not significantly affect our data.

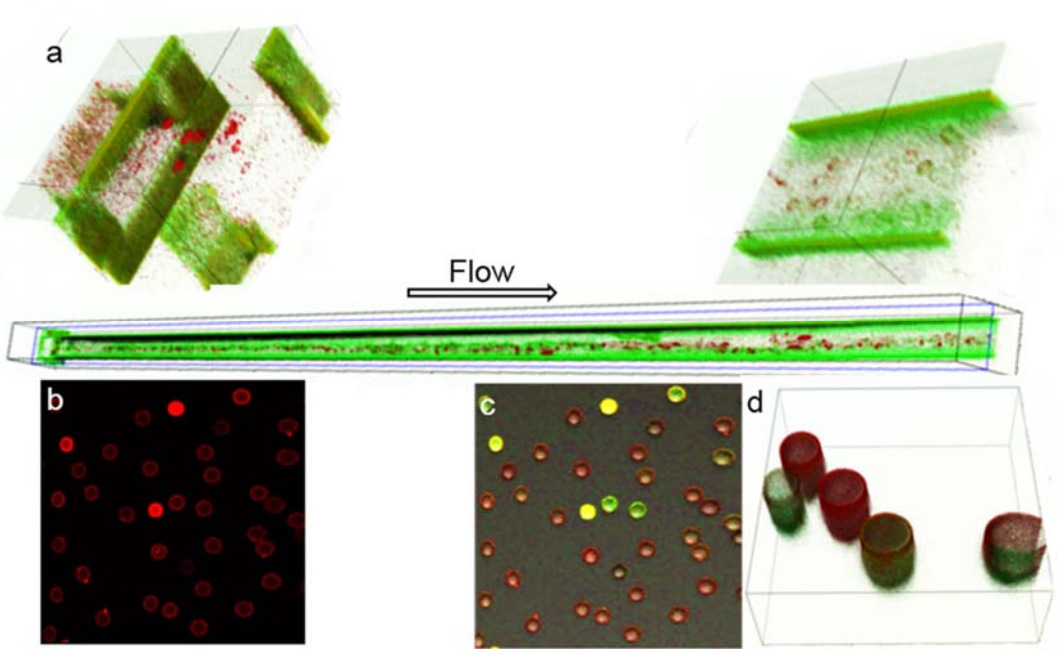

Figure 3. CLSM images of time-resolved protein corona formation. (a) In situ observation of protein corona formation in a dynamic system. Fluorescently labeled silica particles (HSA–Cy5 coating, red) are injected into a MF channel. HSA–Cy3 solution (green) is injected into the side channels at the same time. Near the channel entrance, only the HSA–Cy5 precoating is observed. Toward the channel exit, the particles are additionally coated with HSA–Cy3 (green). Ex situ particle characterization by CLSM: (b) HSA–Cy5-labeled particles prior to incubation. (c, d) Post-incubation images.

Prior to injection, the particles exhibited red fluorescence only, owing to the HSA–Cy5 coating (Figure 3b). After incubation, the particles were coated further with HSA–Cy3 (Figure 3c,d). The same coating trend was observed in situ (Figure 3a). Near the channel entrance, only red fluorescence (HSA–Cy5 precoating) was detected at the particle surfaces, whereas toward the channel exit, two different protein layers were visible (initial HSA–Cy5 coating and secondary HSA–Cy3 coating). These qualitative results indicate that the adsorbed protein layers are stable, and therefore do not desorb, in protein-rich environments. Furthermore, additional protein layers

can adsorb, as indicated by the "layer" build-up. (Figure 3c,d). Quantitative results were obtained from 2D images using the static set-up (Figure 4).

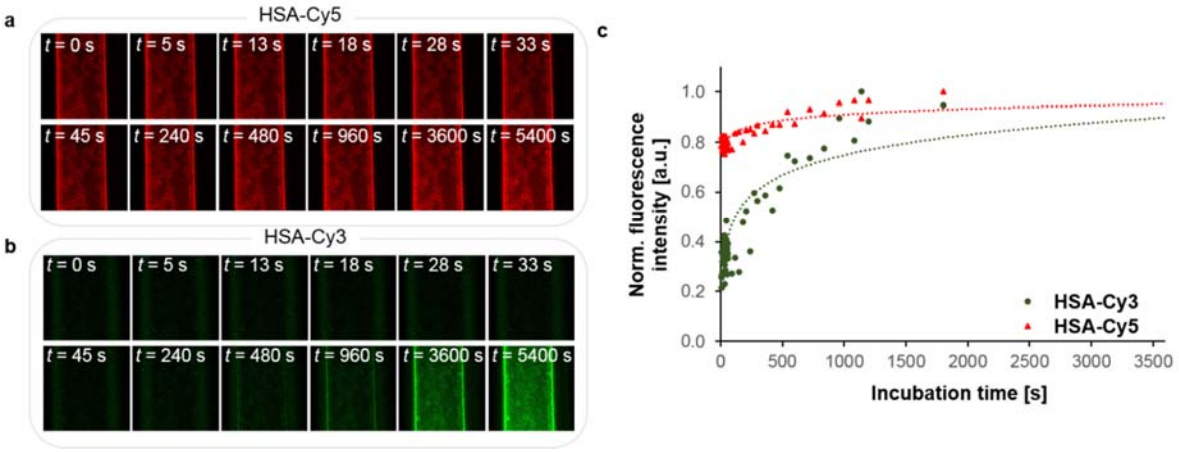

Figure 4. Kinetics of protein corona formation around HSA–Cy5 precoated silica particles. A constant flow rate of 600 μL h^{-1} and an HSA–Cy3 concentration of 0.2 mg mL^{-1} were used. CLSM images of a particle–protein suspension after incubation at different times with HSA–Cy3 captured using (a) 638-nm and (b) 552-nm laser detection. (c) Quantitative data: normalized and background-corrected particle fluorescence intensity plotted against time for both detection channels (the red triangles represent data obtained using a 638-nm laser and green circles represent data obtained using a 552-nm laser).

To distinguish between the initial HSA–Cy5 coating and protein corona formation during incubation (HSA–Cy3), the fluorescence intensities of both protein solutions were detected separately using both the 638-nm (red fluorescence) and 552-nm (green fluorescence) laser channels. The red fluorescence intensity was constant throughout the 90-min incubation process (Figure 4a,c). Note that the slight increase in normalized fluorescence intensity (from 0.8 to 1.0) was due to the overlapping laser intensities (Figure 4c). These results show that a preformed protein corona is stable in protein-rich environments. Incubation led to an increase in the green

fluorescence intensity, indicating that a second protein layer was adsorbed on top of the HSA–Cy5 layer (Figure 4b,c). Generally, the same kinetic features for protein adsorption as observed on bare silica particles (Figure 1) were observed. Fluorescence intensity increased rapidly over the first ca. 40 s, plateaued for ca. 60 s, and increased again until a plateau was reached. These data confirm the qualitative results from the dynamic measurements, that is "hard" protein corona proteins are stable under physiologically relevant conditions and do not prevent the formation of a "second" protein corona. The kinetics data, however, show that adsorption profiles are different when compared with those of the bare silica particles (Table 1), indicating that surface chemistry influences the time-evolution of protein corona formation. Furthermore, non-fluorescently labeled HSA was found to only displace pre-adsorbed Cy5–HSA to a minor extent (Figure S11), indicating that the pre-adsorbed protein corona cannot be significantly competitively displaced by other HSA in solution.

Influence of Particle Surface Chemistry. To further analyze the influence of surface chemistry, we compared bare silica particles with HSA- and zwitterionic polymer-coated silica particles. Zwitterionic polymers are widely used as low-fouling coatings, as they can improve bioavailability owing to their well-hydrated surface.[51–54] A low-fouling coating with PMPC was formed via SI-ATRP of MPC as the main zwitterionic monomer, and HEMA as an additional monomer to obtain a hydroxyl functionality. Prior to polymerization, ATRP initiator groups were attached to the silica surface (Scheme S1). For visualization of the particles by fluorescence microscopy, we conjugated AF488-NHS to all of the HEMA repeating units in the polymer (Figure S12). Protein coating was performed by immersing the silica particles in an HSA solution. Cy5-Functionalized HSA was used instead of non-labeled HSA to fluorescently label the protein-coated particles. Further characterization was conducted using thermogravimetric analysis (Figure S12).

For all experiments, a constant flow rate of 600 µL h^{-1} and a HSA–Cy5 concentration of 0.2 mg mL^{-1} in DPBS were used. Figure 5 shows the quantitative data obtained (the respective raw data for each particle system are displayed in Figure S13a). Note that the data for uncoated silica particles are the same as the graph (replicate no. 2) in Figure 1.

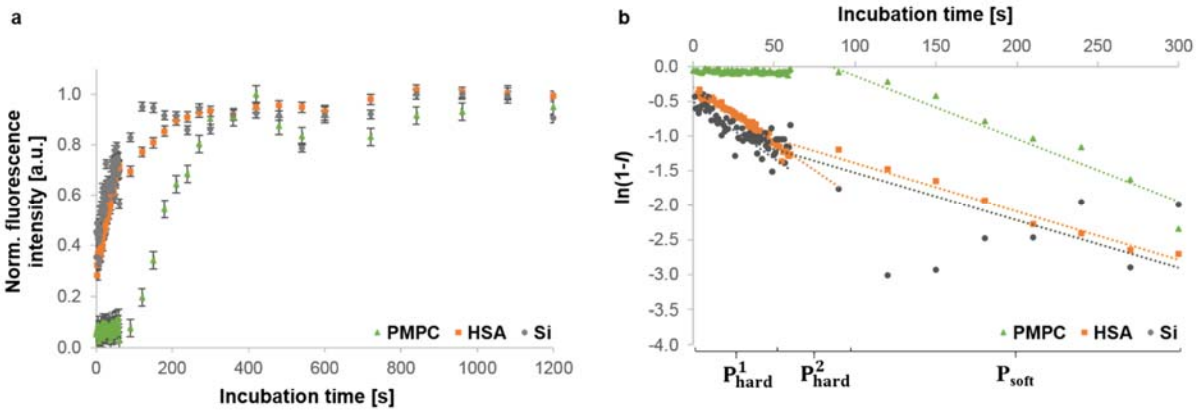

Figure 5. Kinetics of protein corona formation around silica particles with different surface chemistries. (a) Background-corrected, normalized particle fluorescence intensity plotted against incubation time for the bare silica particles, and PMPC- and HSA-coated silica particles (denoted as Si, PMPC, and HSA, respectively). (b) Linearization of the data plotted in (a) with respective linear fits. R^2 values, which indicate goodness-of-fit, and respective equations for the regression lines are summarized in Table S3.

Similar trends for protein adsorption onto HSA-coated particles were observed as those described for the bare silica particles (Figure 1, Table 1): (1) an increase of fluorescence intensity (Figure 5a); (2) division into "hard" and "soft" protein coronas according to the different adsorption rates (Figure 5b, Table 2); and (3) active protein adsorption (P^1_{hard}) to form the "hard" protein corona is 2.5 times faster than "soft" protein corona formation (Table 2). However, (2) and (3) only apply for the HSA-coated and bare silica particles. The fluorescence intensity increased rapidly over the first ca. 40 s for the protein-coated and bare silica particles (formation of P^1_{hard}).

In comparison, the PMPC coating drastically changed the adsorption profile—no increase in fluorescence intensity was detected for the polymer-functionalized particles in the initial stages of incubation. These results suggest that only very few proteins are closely bound to the surface. Specifically, a plateau was observed over the first 60 s of incubation, which we propose to be P^2_{hard} (irreversibly bound proteins, however, not tightly attached to the surface). The τ value confirmed the assignment of this phase to P^2_{hard}, as the calculated adsorption rate was very high (2500 s). These results confirm the low-fouling effect of zwitterionic polymers. Zwitterionic materials prevent proteins from adsorbing by forming a tightly bound water layer around the polymer chains, which acts as a physical and energetic barrier.[55] Similar results were reported by Moyano et al. for sulfobetaine-coated gold nanoparticles, where the absence of irreversibly bound proteins ("hard" protein corona) was reported.[52]

Table 2. Experimental Parameters for the Bare Silica, and PMPC- and HSA-Precoated Particles Obtained from the Data Presented in Figure 5

Coating	Time span P^1_{hard} [s]	Time span P^2_{hard} [s]	Time span P_{soft} [s]	τ_{P1} [s]	τ_{P2} [s]	τ_{soft} [s]	Plateau [s]
None (bare silica particles)	36	23	5340	61	-	145	120
PMPC	-	60	5340	-	2500	110	300
HSA	44	46	5310	63	-	143	270

Influence of Protein Flow Rate. Another aspect of growing interest is the influence of flow on protein corona formation.[56–58] Our system provides a dynamic environment and additionally

allows variation of flow rates. It has been shown that protein corona composition is different for static and dynamic incubation.[39,57–59] However, little is known about the influence of different flow rates on the time-evolution of protein corona formation. Figure 6 shows the results from the MF-CLSM measurements using bare silica particles and HSA–Cy5 as model systems, with applied flow rates of 0, 600, and 1250 µL h^{-1}.

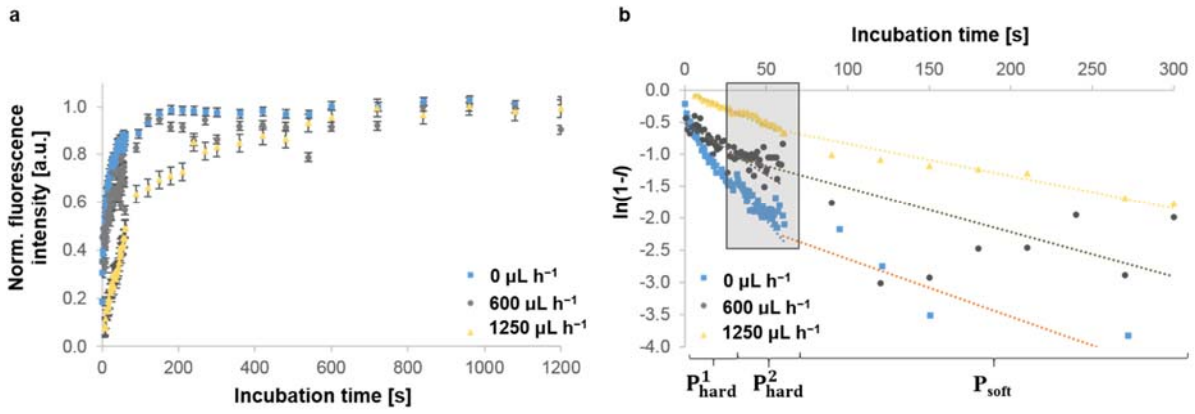

Figure 6. Kinetics of protein corona formation around silica particles at different flow rates. (a) Background-corrected, normalized particle fluorescence intensity plotted against incubation time at varying flow rates. (b) Linearization of the data plotted in (a) with respective linear fits. Raw data are displayed in Figure S13b. R^2 values, which indicate goodness-of-fit, and respective equations for the regression lines are summarized in Table S4.

For each flow rate studied, protein corona formation grew logarithmically (Figure 6a), showing a steep increase in fluorescence intensity over the first ca. 35 s (Table 3) and the formation of a stable plateau after ca. 60 s. The plateau P^2_{hard}, which indicates the transition between "hard" and "soft" protein corona, is much less pronounced at very high (1250 µL h^{-1}) and "static" (0 µL h^{-1}) flow rates when compared with that obtained at an intermediate flow rate (600 µL h^{-1}, Figure 1 (graph replicate no. 2)). Generally, with increasing flow rates, the states of equilibrium, that is, the final plateaus, were reached at later stages (Table 3). Furthermore, the active adsorption steps (τ_{P1},

τ_{soft}) were slower when higher flow rates were applied. These results indicate that protein corona formation occurs at a much slower rate when proteins rapidly flow past the particles (high flow rates). When proteins adsorb onto a surface, they undergo three successive steps: (1) diffusion to the surface; (2) attachment to the surface; and (3) relaxation to reach an equilibrium state.[60]

Table 3. Experimental Parameters for the Bare Silica Particles Incubated in HSA–Cy5 Using Different Applied Flow Rates Obtained from the Data Presented in Figure 6

Flow rate [μL h^{-1}]	Time span P^1_{hard} [s]	Time span P^2_{hard} [s]	Time span P_{soft} [s]	τ_{P1} [s]	τ_{soft} [s]	Plateau [s]
0	41	17	5342	32	112	151
600	36	23	5340	61	145	120
1250	29	13	5358	92	196	360

Influence of Protein Concentration. In addition to surface chemistry and flow rate, protein concentration influences protein corona formation. Studies have shown that with increasing serum concentrations, the adsorbed protein mass increases.[61,62] However, a detailed understanding of the full effects of protein concentration on the kinetics of protein corona formation on the surface of spherical microparticles has yet to be established. Herein, we studied the influence of HSA–Cy5 concentration (0.1, 0.2, and 0.4 mg mL^{-1}) on the time-evolution of protein corona formation on bare silica particles (Figure S14, Table S5). The three different phases of protein corona formation were observed for each data set. However, there was no clear trend evident from varying the HSA–Cy5 concentration (Table S6). This may suggest that a very small amount (<0.1 mg mL^{-1}) of protein is sufficient to form a stable protein corona around microparticles. The highest protein concentration studied (0.4 mg mL^{-1}) resulted in low τ values for the active adsorption steps (τ_{P1} =

20 s, τ_{soft} = 29 s), indicating very fast adsorption rates—also, a 14 s time span was obtained for formation of the initial plateau. We hypothesize that, besides a lower limit, there might be an upper limit of protein concentration that still allows the different phases to be distinguished.

The present technique is a versatile and accurate approach to study different aspects of protein corona formation in situ. It provides important insights into the time-evolution of protein corona formation and allows clear distinction between different protein layers. We showed the existence of the "soft" protein corona, even for low-fouling materials, and examined the adsorption kinetics for corona formation. The interaction of more complex mixtures with particles, such as multi-protein systems with different fluorescent labels, is the subject of future investigations. The defined incubation environment with controlled parameters (e.g., chip geometry, flow rate, incubation time) may allow standardization of experiments, which would enable interlaboratory comparisons of data, potentially leading to the prediction of protein corona formation.

CONCLUSIONS

In summary, we introduced the combination of CLSM with MF as a technique to study the time-evolution of protein corona formation in situ. Linearization of the experimental data led to a characteristic time that is directly related to adsorption rate. We suggested a three-phase model for protein corona formation: a tightly, irreversibly bound layer of proteins that is directly adsorbed onto the particle surface (phase 1), an intermediate layer wherein the proteins are not directly attached to the surface, but still irreversibly bound and therefore belonging to the inner "hard" protein corona (phase 2), and an outer protein layer, the "soft" protein corona, consisting of reversibly bound proteins (phase 3). Measurements concerning the stability of a preformed protein corona showed that pre-adsorbed proteins were stable under physiological conditions and, once incubated in protein-containing solutions, formed a "second" protein corona. Furthermore, we

showed that low-fouling zwitterionic surface coatings prevented the adsorption of tightly bound proteins but formed a “soft” protein corona. A comparison of the effect of different flow rates showed that higher flow rates led to slower adsorption kinetics, whereas protein concentrations minimally influenced the adsorption rate. Additionally, we presented preliminary data of microfluidics in combination with high-speed camera imaging. This set-up allowed detailed insights on very small time scales (~0.5 s) of protein corona formation. Forthcoming studies will focus on the combination of microfluidics with Raman spectroscopy to overcome limitations of using fluorescently labeled protein solutions and therefore broaden the applicability range to non-fluorescently labeled solutions. Using high-resolution microscopy may extend the applicability of the present technique to smaller particles that are below the detection limit of standard confocal laser scanning microscopes. However, a thinner chip design would be needed.

ASSOCIATED CONTENT

Supporting Information. Theoretical and experimental details of the kinetic studies.

AUTHOR INFORMATION

Corresponding Author

*E-mail: fcaruso@unimelb.edu.au.

Author Contributions

A.C.G.W. and Q.A.B. designed and performed the experiments, analyzed and interpreted the data, and wrote the paper, K. Krüger assisted with the high-speed camera imaging and CLSM image analysis, M.S. assisted with designing the experiments and the CLSM measurements, and K. Kempe, S.F., and F.C. supervised the studies and edited the paper.

ORCID

Alessia C. G. Weiss: 0000-0001-7274-551X

Kilian Krüger: 0000-0002-2959-5330

Quinn A. Besford: 0000-0002-1779-9176

Mathias Schlenk: 0000-0002-9608-993X

Kristian Kempe: 0000-0002-0136-9403

Stephan Förster: 0000-0002-7323-2449

Frank Caruso: 0000-0002-0197-497X

Notes

The authors declare no competing financial interest.

ACKNOWLEDGMENT

This research was conducted and funded by the Australian Research Council (ARC) Centre of Excellence in Convergent Bio-Nano Science and Technology (Project No. CE140100036). K. Kempe and F.C. acknowledge the awards of a National Health and Medical Research Council (NHMRC)–ARC Dementia Research Development Fellowship (APP1109945) and an NHMRC Senior Principal Research Fellowship (APP1135806), respectively. A.C.G.W. acknowledges funding from The University of Melbourne through Melbourne International Research Scholarship. This work was also supported by the European Research Council (ERC)–Advanced Grant STREAM (project 291211). The authors also acknowledge financial support by the German Academic Exchange Service (DAAD) through its Thematic network Bayreuth-Melbourne

Colloid/Polymer Network sponsored from funds of the Federal Ministry of Education and Research (BMBF). We acknowledge F. Akgök, R. Suckfüll, and M. Faria for assistance with measurements.

REFERENCES

1. Lin, S.; Mortimer, M.; Chen, R.; Kakinen, A.; Riviere, J.; Davis, T. P.; Ding, F.; Ke, P. C. NanoEHS Beyond Toxicity – Focusing on Biocorona. *Environ. Sci.: Nano* **2017**, *4*, 1433–1454.

2. Caracciolo, G.; Farokhzad, O. C.; Mahmoudi, M. Biological Identity of Nanoparticles In Vivo: Clinical Implications of the Protein Corona. *Trends Biotechnol.* **2016**, *35*, 257–264.

3. Schubert, J.; Chanana, M. Coating Matters: Review on Colloidal Stability of Nanoparticles with Biocompatible Coatings in Biological Media, Living Cells and Organisms. *Curr. Med. Chem.* **2018**, DOI: 10.2174/0929867325666180601101859.

4. Hadjidemetriou, M.; Kostarelos, K. Nanomedicine: Evolution of the Nanoparticle Corona. *Nat. Nanotechnol.* **2017**, *12*, 288–290.

5. Lundqvist, M.; Stigler, J.; Elia, G.; Lynch, I.; Cedervall, T.; Dawson, K. A. Nanoparticle Size and Surface Properties Determine the Protein Corona with Possible Implications for Biological Impacts. *Proc. Natl. Acad. Sci. U. S. A.* **2008**, *105*, 14265–14270.

6. Docter, D.; Westmeier, D.; Markiewicz, M.; Stolte, S.; Knauer, S. K.; Stauber, R. H. The Nanoparticle Biomolecule Corona: Lessons Learned – Challenge Accepted? *Chem. Soc. Rev.* **2015**, *44*, 6094–6121.

7. Pederzoli, F.; Tosi, G.; Vandelli, M. A.; Belletti, D.; Forni, F.; Ruozi, B. Protein Corona and Nanoparticles: How Can We Investigate on? *Wiley Interdiscip. Rev.: Nanomed. Nanobiotechnol.* **2017**, e1467.

8. Walkey, C. D.; Chan, W. C. Understanding and Controlling the Interaction of Nanomaterials with Proteins in a Physiological Environment. *Chem. Soc. Rev.* **2012**, *41*, 2780–2799.

9. Kim, J.-H.; Yoon, J.-Y. Protein Adsorption on Polymer Particles. *Encycl. Surf. Colloid Sci.* **2002**, *1*, 4373–4381.

10. Norde, W.; Lyklema, J. Protein Adsorption and Bacterial Adhesion to Solid Surfaces – A Colloid-Chemical Approach. *Colloids Surf.* **1989**, *38*, 1–13.

11. Norde, W. Energy and Entropy of Protein Adsorption. *J. Dispersion Sci. Technol.* **2007**, *13*, 363–377.

12. Milani, S.; Bombelli, F. B.; Pitek, A. S.; Dawson, K. A.; Rädler, J. Reversible Versus Irreversible Binding of Transferrin to Polystyrene Nanoparticles: Soft and Hard Corona. *ACS Nano* **2017**, *6*, 2532–2541.

13. Del Pino, P.; Pelaz, B.; Zhang, Q.; Maffre, P.; Nienhaus, G. U.; Parak, W. J. Protein Corona Formation around Nanoparticles – from the Past to the Future. *Mater. Horiz.* **2014**, *1*, 301–313.

14. Peng, Q.; Mu, H. The Potential of Protein–Nanomaterial Interaction for Advanced Drug Delivery. *J. Controlled Release* **2016**, *225*, 121–132.

15. Sund, J.; Alenius, H.; Vippola, M.; Savolainen, K.; Puustinen, A. Proteomic Characterization of Engineered Nanomaterial–Protein Interactions in Relation to Surface Reactivity. *ACS Nano* **2011**, *5*, 4300–4309.

16. Lynch, I.; Cedervall, T.; Lundqvist, M.; Cabaleiro-Lago, C.; Linse, S.; Dawson, K. A. The Nanoparticle–Protein Complex as a Biological Entity; A Complex Fluids and Surface Science Challenge for the 21st Century. *Adv. Colloid Interface Sci.* **2007**, *134–135*, 167–174.

17. Lundqvist, M.; Stigler, J.; Cedervall, T.; Berggård, T.; Flanagan, M. B.; Lynch, I.; Elia, G.; Dawson, K. The Evolution of the Protein Corona around Nanoparticles: A Test Study. *ACS Nano* **2011**, *5*, 7503–7509.

18. Sakulkhu, U.; Mahmoudi, M.; Maurizi, L.; Salaklang, J.; Hofmann, H. Protein Corona Composition of Superparamagnetic Iron Oxide Nanoparticles with Various Physico-Chemical Properties and Coatings. *Sci. Rep.* **2014**, *4*, 5020.

19. Chanana, M.; Rivera_Gil, P.; Correa-Duarte, M. A.; Liz-Marzán, L. M.; Parak, W. J. Physicochemical Properties of Protein-Coated Gold Nanoparticles in Biological Fluids and Cells before and after Proteolytic Digestion. *Angew. Chem., Int. Ed.* **2013**, *52*, 4179–4183.

20. Zanganeh, S.; Spitler, R.; Erfanzadeh, M.; Alkilany, A. M.; Mahmoudi, M. Protein Corona: Opportunities and Challenges. *Int. J. Biochem. Cell Biol.* **2016**, *75*, 143–147.

21. Mahmoudi, M. Protein Corona: The Golden Gate to Clinical Applications of Nanoparticles. *Int. J. Biochem. Cell Biol.* **2016**, *75*, 141–142.

22. Foroozandeh, P.; Aziz, A. A. Merging Worlds of Nanomaterials and Biological Environment: Factors Governing Protein Corona Formation on Nanoparticles and Its Biological Consequences. *Nanoscale Res. Lett.* **2015**, *10*, 221.

23. Shang, L.; Nienhaus, G. U. In Situ Characterization of Protein Adsorption onto Nanoparticles by Fluorescence Correlation Spectroscopy. *Acc. Chem. Res.* **2017**, *50*, 387–395.

24. Mahmoudi, M.; Lynch, I.; Ejtehadi, M. R.; Monopoli, M. P.; Bombelli, F. B.; Laurent, S. Protein–Nanoparticle Interactions: Opportunities and Challenges. *Chem. Rev.* **2011**, *111*, 5610–5637.

25. Wang, H.; Shang, L.; Maffre, P.; Hohmann, S.; Kirschhöfer, F.; Brenner-Weiss, G.; Nienhaus, G. U. The Nature of a Hard Protein Corona Forming on Quantum Dots Exposed to Human Blood Serum. *Small* **2016**, *12*, 5836–5844.

26. Pisani, C.; Gaillard, J. C.; Dorandeu, C.; Charnay, C.; Guari, Y.; Chopineau, J.; Devoisselle, J. M.; Armengaud, J.; Prat, O. Experimental Separation Steps Influence the Protein Content of Corona around Mesoporous Silica Nanoparticles. *Nanoscale* **2017**, *9*, 5769–5772.

27. Casals, E.; Pfaller, T.; Duschl, A.; Oostingh, G. J.; Puntes, V. Time Evolution of the Nanoparticle Protein Corona. *ACS Nano* **2010**, *4*, 3623–3632.

28. Schäffler, M.; Semmler-Behnke, M.; Sarioglu, H.; Takenaka, S.; Wenk, A.; Schleh, C.; Hauck, S. M.; Johnston, B. D.; Kreyling, W. G. Serum Protein Identification and Quantification of the Corona of 5, 15 and 80 nm Gold Nanoparticles. *Nanotechnology* **2013**, *24*, 265103.

29. Lacerda, S. H. D. P.; Park, J. J.; Meuse, C.; Pristinski, D.; Becker, M. L.; Karim, A.; Douglas, J. F. Interaction of Gold Nanoparticles with Common Human Blood Proteins. *ACS Nano* **2010**, *4*, 365–379.

30. Kaufman, E. D.; Belyea, J.; Johnson, M. C.; Nicholson, Z. M.; Ricks, J. L.; Shah, P. K.; Bayless, M.; Pettersson, T.; Feldötö, Z.; Blomberg, E.; Claesson P.; Franzen S. Probing Protein Adsorption onto Mercaptoundecanoic Acid Stabilized Gold Nanoparticles and Surfaces by Quartz Crystal Microbalance and ʒ-Potential Measurements. *Langmuir* **2007**, *23*, 6053–6062.

31. Mahmoudi, M.; Shokrgozar, M. A.; Sardari, S.; Moghadam, M. K.; Vali, H.; Laurent, S.; Stroeve, P. Irreversible Changes in Protein Conformation Due to Interaction with Superparamagnetic Iron Oxide Nanoparticles. *Nanoscale* **2011**, *3*, 1127–1138.

32. Lehman, S. E.; Mudunkotuwa, I. A.; Grassian, V. H.; Larsen, S. C. Nano–Bio Interactions of Porous and Nonporous Silica Nanoparticles of Varied Surface Chemistry: A Structural, Kinetic, and Thermodynamic Study of Protein Adsorption from RPMI Culture Medium. *Langmuir* **2016**, *32*, 731–742.

33. Cedervall, T.; Lynch, I.; Lindman, S.; Berggård, T.; Thulin, E.; Nilsson, H.; Dawson, K. A.; Linse, S. Understanding the Nanoparticle–Protein Corona Using Methods to Quantify Exchange Rates and Affinities of Proteins for Nanoparticles. *Proc. Natl. Acad. Sci. U. S. A.* **2007**, *104*, 2050–2055.

34. Björnmalm, M.; Faria, M.; Caruso, F. Increasing the Impact of Materials in and beyond Bio-Nano Science. *J. Am. Chem. Soc.* **2016**, *138*, 13449–13456.

35. Mulvaney, P.; Wolfgang, P. J.; Caruso, F. Weiss, P. S. Standardizing Nanomaterials. *ACS Nano* **2016**, *10*, 9763–9764.

36. Polacheck, W. J.; Li, R.; Uzel, S. G.; Kamm, R. D. Microfluidic Platforms for Mechanobiology. *Lab Chip* **2013**, *13*, 2252–2267.

37. Trebbin, M.; Krüger, K.; DePonte, D.; Roth, S. V.; Chapman, H. N.; Förster, S. Microfluidic Liquid Jet System with Compatibility for Atmospheric and High-Vacuum Conditions. *Lab Chip* **2014**, *14*, 1733–1745.

38. Müllner, M.; Cui, J.; Noi, K. F.; Gunawan, S. T.; Caruso, F. Surface-Initiated Polymerization within Mesoporous Silica Spheres for the Modular Design of Charge-Neutral Polymer Particles. *Langmuir* **2014**, *30*, 6289–6293.

39. Weiss, A. C. G.; Kempe, K.; Förster, S.; Caruso, F. Microfluidic Examination of the "Hard" Biomolecular Corona Formed on Engineered Particles in Different Biological Milieu. *Biomacromolecules* **2018**, *19*, 2580–2594.

40. Qin, D.; Xia, Y.; Whitesides, G. M. Soft Lithography for Micro- and Nanoscale Patterning. *Nat. Protoc.* **2010**, *5*, 491–502.

41. Vennemann, P.; Lindken, R.; Westerweel, J. In Vivo Whole-Field Blood Velocity Measurement Techniques. *Exp. Fluids* **2007**, *42*, 495–511.

42. Welter, M.; Rieger, H. Interstitial Fluid Flow and Drug Delivery in Vascularized Tumors: A Computational Model. *PLoS One* **2013**, *8*, e70395–e70418.

43. Tenzer, S.; Docter, D.; Kuharev, J.; Musyanovych, A.; Fetz, V.; Hecht, R.; Schlenk, F.; Fischer, D.; Kiouptsi, K.; Reinhardt, C.; Landfester, K.; Schild, H.; Maskos, M.; Knauer, S. K.;

Stauber, R. H. Rapid Formation of Plasma Protein Corona Critically Affects Nanoparticle Pathophysiology. *Nat. Nanotechnol.* **2013**, *8*, 772–781.

44. Schöttler, S.; Becker, G.; Winzen, S.; Steinbach, T.; Mohr, K.; Landfester, K.; Mailänder, V.; Wurm, F. R. Protein Adsorption is Required for Stealth Effect of Poly(ethylene glycol)- and Poly(phosphoester)-Coated Nanocarriers. *Nat. Nanotechnol.* **2016**, *11*, 372–377.

45. Clemments, A. M.; Botella, P.; Landry, C. C. Spatial Mapping of Protein Adsorption on Mesoporous Silica Nanoparticles by Stochastic Optical Resolution Microscopy. *J. Am. Chem. Soc.* **2017**, *139*, 3978–3981.

46. Kastantin, M.; Langdon, B. B.; Schwartz, D. K. A Bottom-Up Approach to Understanding Protein Layer Formation at Solid–Liquid Interfaces. *Adv. Colloid Interface Sci.* **2014**, *207*, 240–252.

47. Rabe, M.; Verdes, D.; Seeger, S. Understanding Protein Adsorption Phenomena at Solid Surfaces. *Adv. Colloid Interface Sci.* **2011**, *162*, 87–106.

48. Pomorska, A.; Adamczyk, Z.; Nattich-Rak, M.; Sadowska, M. Kinetics of Human Serum Albumin Adsorption at Silica Sensor: Unveiling Dynamic Hydration Function. *Colloids Surf., B* **2018**, *167*, 377–384.

49. Nattich-Rak, M.; Sadowska, M.; Adamczyk, Z.; Cieśla, M.; Kąkol, M. Formation Mechanism of Human Serum Albumin Monolayers on Positively Charged Polymer Microparticles. *Colloids Surf., B* **2017**, *159*, 929–936.

50. Zhang, H.; Peng, J.; Li, X.; Liu, S.; Hu, Z.; Xu, G.; Wu, R. A Nano-Bio Interfacial Protein Corona on Silica Nanoparticle. *Colloids Surf., B* **2018**, *167*, 220–228.

51. Leng, C.; Hung, H. C.; Sun, S.; Wang, D.; Li, Y.; Jiang, S.; Chen, Z. Probing the Surface Hydration of Nonfouling Zwitterionic and PEG Materials in Contact with Proteins. *ACS Appl. Mater. Interfaces* **2015**, *7*, 16881–16888.

52. Moyano, D. F.; Saha, K.; Prakash, G.; Yan, B.; Kong, H.; Yazdani, M.; Rotello, V. M. Fabrication of Corona-Free Nanoparticles with Tunable Hydrophobicity. *ACS Nano* **2014**, *8*, 6748–6755.

53. García, K. P.; Zarschler, K.; Barbaro, L.; Barreto, J. A.; O'Malley, W.; Spiccia, L.; Stephan, H.; Graham, B. Zwitterionic-Coated "Stealth" Nanoparticles for Biomedical Applications: Recent Advances in Countering Biomolecular Corona Formation and Uptake by the Mononuclear Phagocyte System. *Small* **2014**, *10*, 2516–2529.

54. Photos, P. J.; Bacakova, L.; Discher, B.; Bates, F. S.; Discher, D. E. Polymer Vesicles In Vivo: Correlations with PEG Molecular Weight. *J. Controlled Release* **2003**, *90*, 323–334.

55. Chen, S.; Li, L.; Zhao, C.; Zheng, J. Surface Hydration: Principles and Applications toward Low-Fouling/Nonfouling Biomaterials. *Polymer* **2010**, *51*, 5283–5293.

56. Braun, N. J.; DeBrosse, M. C.; Hussain, S. M.; Comfort, K. K. Modification of the Protein Corona–Nanoparticle Complex by Physiological Factors. *Mater. Sci. Eng., C* **2016**, *64*, 34–42.

57. Palchetti, S.; Colapicchioni, V.; Digiacomo, L.; Caracciolo, G.; Pozzi, D.; Capriotti, A. L.; La Barbera, G.; Laganà, A. The Protein Corona of Circulating PEGylated Liposomes. *Biochim. Biophys. Acta* **2016**, *1858*, 189–196.

58. Pozzi, D.; Caracciolo, G.; Digiacomo, L.; Colapicchioni, V.; Palchetti, S.; Capriotti, A. L.; Cavaliere, C.; Zenezini Chiozzi, R.; Puglisi, A.; Laganà, A. The Biomolecular Corona of Nanoparticles in Circulating Biological Media. *Nanoscale* **2015**, *7*, 13958–13966.

59. Palchetti, S.; Pozzi, D.; Capriotti, A. L.; La Barbera, G.; Chiozzi, R. Z.; Digiacomo, L.; Peruzzi, G.; Caracciolo, G; Laganà, A. Influence of Dynamic Flow Environment on Nanoparticle–Protein Corona: From Protein Patterns to Uptake in Cancer Cells. *Colloids Surf., B* **2017**, *153*, 263–271.

60. Salari, A.; Kumacheva, E. Microfluidic Studies of Polymer Adsorption in Flow. *Macromol. Chem. Phys.* **2017**, *218*, 1600328.

61. Gräfe, C.; Weidner, A.; Lühe, M. V.; Bergemann, C.; Schacher, F. H.; Clement, J. H.; Dutz, S. Intentional Formation of a Protein Corona on Nanoparticles: Serum Concentration Affects Protein Corona Mass, Surface Charge, and Nanoparticle–Cell Interaction. *Int. J. Biochem. Cell Biol.* **2015**, *75*, 196–202.

62. Caracciolo, G.; Pozzi, D.; Capriotti, A. L.; Cavaliere, C.; Foglia, P.; Amenitsch, H.; Laganà, A. Evolution of the Protein Corona of Lipid Gene Vectors as a Function of Plasma Concentration. *Langmuir* **2011**, *27*, 15048–15053.

For Table of Contents use only

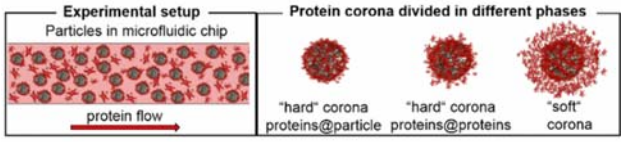

Author/s:
Weiss, ACG; Krueger, K; Besford, QA; Schlenk, M; Kempe, K; Foerster, S; Caruso, F

Title:
In Situ Characterization of Protein Corona Formation on Silica Microparticles Using Confocal Laser Scanning Microscopy Combined with Microfluidics

Date:
2019-01-16

Citation:
Weiss, A. C. G., Krueger, K., Besford, Q. A., Schlenk, M., Kempe, K., Foerster, S. & Caruso, F. (2019). In Situ Characterization of Protein Corona Formation on Silica Microparticles Using Confocal Laser Scanning Microscopy Combined with Microfluidics. ACS APPLIED MATERIALS & INTERFACES, 11 (2), pp.2459-2469. https://doi.org/10.1021/acsami.8b14307.